Rowan University

# Rowan Digital Works

3-24-2014

# Assessing the transport of receptor-mediated drug-delivery devices across cellular monolayers

Erik Brewer
*Rowan University*

Anthony Lowman
*Rowan University*

Follow this and additional works at: https://rdw.rowan.edu/engineering_facpub

 Part of the Biomedical Engineering and Bioengineering Commons, Biophysics Commons, Nanotechnology Commons, and the Organic Chemistry Commons

## Recommended Citation

# Assessing the transport of receptor-mediated drug-delivery devices across cellular monolayers

**Erik Brewer**[a] and **Anthony M. Lowman**[b]

[a]Drexel University, 3201 Chestnut Street, Philadelphia, PA 19104 USA

[b]Rowan University, 201 Mullica Hill Rd Glassboro, NJ 08028 USA

## Abstract

Receptor-mediated endocytosis (RME) has been extensively studied as a method for augmenting the transport of therapeutic devices across monolayers. These devices range from simple ligand-therapeutic conjugates to complex ligand-nanocarrier systems. However, characterizing the uptake of these carriers typically relies on their comparisons to the native therapeutic, which provides no understanding of ligand or cellular performance. To better understand the potential of the RME pathway, a model for monolayer transport was designed based on the endocytosis cycle of transferrin, a ligand often used in RME drug-delivery devices. This model established the correlation between apical receptor concentration and transport capability. Experimental studies confirmed this relationship, demonstrating an upper transport limit independent of the applied dose. This contrasts with the dose-proportional pathways native therapeutics rely on for transport. Thus, the direct comparison of these two transport mechanisms can produce misleading results that change with arbitrarily chosen doses. Furthermore, transport potential was hindered by repeated use of the RME-cycle. Future studies should base the success of this technology not on the performance of the therapeutic itself, but on the capabilities of the cell. Using receptor-binding studies, we were able to demonstrate how these capabilities can be predicted and potentially adopted for high-throughput screening methods.

### Keywords

Monolayer; Receptors; Drug delivery systems; Passive diffusion/transport; Targeted drug delivery; Active transport; Endocytosis

## 1. Introduction

Ligand-receptor interactions have long been utilized for drug delivery systems due to a number of beneficial traits they possess: therapeutics utilizing this interaction circumvent P-glycoprotein (P-gp) efflux transporters, the key mechanism responsible for multi-drug resistance; their high specificity allows for site-specific targeting; the ligands illicit low immunological responses; and receptor-mediated endocytosis (RME) permits intra- and transcellular passage of large molecules which would normally be prevented from

Corresponding author: Erik Brewer, Department of Chemical Engineering, Drexel University, 3201 Chestnut Street, Philadelphia, PA 19104 USA, ecb34@drexel.edu, Tel: +1-215-895-2227, Fax: +1-215-895-5837.

permeating the cell wall[1–3]. Drug-delivery and nanomedical devices tethered to ligands have successfully taken advantages of these traits in a variety of applications: nanoparticles coated with cancer-specific ligands have been used to image early and developed tumours and detect peripheral metastases[4–6]; therapeutics have been directed to target cell-specific receptors to achieve localized delivery[7–9]; chemotherapeutic and gene transfection agents are made more effective when delivered within the intracellular endosomal pathway[9–14].

RME has also been extensively studied as an alternate route across cell monolayers barriers, like those found in the gastrointestinal (GI) tract and the blood-brain barrier (BBB)[15, 16]. The cells that make up these monolayers are joined by tight junctions, forming a continuous wall that limits the diffusion of protein therapeutics due to their low lipid solubility and high molecular size, resulting in their poor bioavailability[17]. RME offers an attractive alternate route that relies on energy driven processes of the cell to transport the therapeutic.

The success of therapeutic-ligand conjugates and therapeutic nanocarrier-ligand devices have been reported using a variety of assessment methods. *In vitro* studies often describe the ability of drugs to traverse these monolayers by measuring the apparent permeability, $P_{app}$, a measure of the transcellular flux normalized with respect to the initial dose and monolayer surface area[18–20]. A more simple analysis, but also dose-normalized, is to report the percentage of the initial dose transported[21]. More absolute measurements report the total accumulation of the conjugate or nanoparticles across the monolayer[18, 22, 23]. *In vivo* measurements mirror many of the latter examples, such as percent transported and drug accumulation[24–26]. More often, the response of the drug is measured, rather than the drug directly, which introduces many specialized assessment methods[27–29]. In oral delivery, RME-devices are often assessed on their bioavailability, a ratio of the oral dose area-under-the-curve (AUC) to the intra-venous AUC, both normalized to their respective doses[23, 30, 31].

Normalizing the transport or response of a therapeutic, as seen in the $P_{app}$, the percent transported, and in the bioavailability, is useful in cases where poor permeability is expected and higher drug concentrations are required to obtain a measurable response[32]. It also allows for comparisons across a variety of experimental methods. In all cases, the RME-drug systems are compared to the transport of the native drug, the non-targeted nanoparticle, or both, to show the improvement on the delivery method. This helps answer the question "how well do these devices improve the uptake or response of the therapeutic?" However, the therapeutics in these cases are simply cargo traveling with the ligand, and the relative efficacy of a drug compared to the drug travelling along these pathways gives no indication of ligand performance or potential. Therefore, we propose an alternative question: "What are the transport capabilities of the RME pathway?"

To answer this, we evaluated the performance of a representative ligand, transferrin (Tf), within the context of therapeutic monolayer transport. A mathematical model of Tf transport was adapted from existing models and kinetic data in literature to help understand the parameters important to transcytosis. We hypothesize that determining the benchmark for successful ligand uptake will help determine the capabilities for further usage in drug delivery devices and expose the limitations of currently used evaluation methods.

## 2. Materials and Methods

### 2.1 Materials

Anti-rabbit transferrin antibody was purchased from Polysciences, Inc. (Warrington, PA). Human transferrin (Tf) and all other chemical reagents were purchased from Sigma Chemical Co. (St. Louis, MO). Non-reagent components were purchased from Fisher Scientific (Pittsburgh, PA).

Tf-iron saturation was performed according to the method developed by Klausner et al.[33] and confirmed using a Tecan Infinite M500 plate reader (Männedorf, Switzerland). All samples with an $A_{465}/A_{280}$ ratio above 0.045 were considered iron-saturated. Biotinylation was achieved using the NHS-biotin reagent, as outlined previously[34]. Briefly, Tf was dissolved in a phosphate buffer (0.1M sodium phosphate, 0.15M NaCl, pH 7.5) at 5mg/ml. NHS-Biotin was added at a 15x molar excess and reacted for 60min at room temperature. The reaction was then purified using gel filtration columns. Biotin content was analyzed using the HABA assay[35] and typically ranged from 3–5mol biotin/mol Tf.

Buffers and components for cell culture media were obtained from Invitrogen (Green Island, New York), with the exception of fetal bovine serum (FBS), which was obtained from Gemini Bio-Products (West Sacramento, California). Growth media consisted of Dulbecco's Modified Eagle Medium (DMEM) with 10% FBS and 1% non-essential amino acids, except where noted.

### 2.2 Cell culture

All experiments were performed using CaCo-2 cells obtained from Sigma Aldrich with passage number ranging from 45–55. Cells were grown until reaching 80% confluency, after which they were collected for the binding studies or seeded for the transport studies. For the transport studies, 12-well Corning (Tewksbury, Massachusetts) Transwell® plates with 0.4μm pores were seeded with approximately 50,000 cells. Cells were fed every other or third day. Tight junction development was monitored by measuring the trans-epithelial electrical resistance (TEER) with an epithelial voltohmmeter (EVOM2, World Precision Instruments, West Haven, CT). TEER values typically plateaued after three weeks, around 800 $\Omega \cdot cm^2$, indicating fully developed tight junctions.

### 2.3 Kinetic and Binding Sites Analysis

Kinetic binding data was obtained according to the procedure outlined by Vieira[36]. Briefly, various concentrations of Tf-biotin were incubated with CaCo-2 cells at 4°C in a HEPES buffer (20mM HEPES-NaOH, 100mM NaCl, 0.1% BSA, pH 7.5) until receptor binding reached equilibrium, about 4hrs. A low temperatures buffer was used to halt the endocytosis cycle and ensure only surface-bound receptors were counted[37]. Control samples, representing binding not specific to the Tf receptor, received a 100x molar excess of unlabeled Tf. The cells were then quickly centrifuged and washed repeatedly with ice-cold buffer, until no un-bound Tf remained. The cells were then treated with a lysing solution (1mM EDTA, 50mM NaCl, 10mM Tris-HCl, 0.1% SDS, 1% Triton X-100, 0.2% BSA, pH 7.4). The lysate solution was then analyzed using the avidin/biotin ELISA assay

outlined in the same procedure to determine bound Tf. Specific binding, or binding associated with the Tf receptor, was calculated from the difference between total binding and control samples.

The association constant and binding-site density were calculated using non-linear regression analysis using the following model[38, 39]:

$$Y = \frac{B_{max} \cdot X}{X + \frac{1}{K_a}} \quad \text{Eq. 1}$$

Here, $Y$ represents the amount of receptor-bound Tf, $X$ the concentration of total Tf in the incubation media, $B_{max}$ the concentration of binding sites, and $K_a$ the association constant.

## 2.4 Transport Studies

Prior to the start of transport studies, culture media were removed from the Transwell® trays and the wells washed three times with Hanks Buffered Saline Solution (HBSS). The cells were then incubated with HBSS for 1hr to deplete intracellular Tf levels leftover from the serum, after which the buffer was then removed. Fresh HBSS was added to the basolateral chamber of the wells, while HBSS with Tf-biotin was added to the apical side. Apical concentrations were 1μg/ml, 10μg/ml or 50 μg/ml. Control samples representing non-specific transport contained a 100x molar excess of unlabeled Tf. Samples were then taken at 30min, 60min, 90min, 120min, 180min, and 240min time points, with fresh HBSS added to replenish the sampled amount. The studies were completed at 37°C. Specific transport, or transport associated exclusively with the Tf-receptor pathway, was calculated from the difference between the total transport and control samples.

Short-term repeat dose studies were conducted to mimic doses given in quick succession, and were performed as follows: transport trays were incubated with HBSS containing 10μg/ml Tf-biotin for 4hrs, to mimic a transport study, although no samples were taken. The cells were then washed three times and incubated with growth media for 2hrs. The cells were washed again, incubated with HBSS for 1hr, and washed a final time. The transport study was then conducted as previously described. Long-term studies were conducted to mimic continual use of the Tf pathways. To accomplish this, cells seeded on Transwell® plates were fed with growth media supplemented with Tf at a concentration at 10μg/ml during the period of tight junction development, approximately 3 weeks. A repeat of the 10μg/ml transport study was then conducted. A complimentary scatchard study was performed on cells grown continuously for the same period with the same modified growth media.

## 2.5 Statistical Analysis

The results of each study are reported and plotted as the mean ± one standard deviation. Statistical differences were determined using ANOVA followed by post-hoc analyses, where $p$ values of $<0.05$ were considered significant.

## 3. Adaptation of Transport Model

One of the most commonly used approaches for modeling biological systems is to outline discrete steps in terms of ordinary differential equations (ODEs)[40]. This method is widely used to describe the receptor-mediated process, with notable examples seen in studies involving the transferrin receptor[41], folic acid[42], low-density lipoprotein[43, 44], and epidermal growth factor (EGF)[45, 46]. Such models vary in complexity depending on their intended use. Detailed models, such as those for EGF which outline 25 or even 125 discrete steps[47, 48], provide a comprehensive and systematic understanding of the biomechanics of an entire ligand-receptor cycle. However, the large number of fitting parameters required in these cases tend to result in poorer performance in pharmacokinetic analyses, which prefer reduced models[49]. In the case of EGF, many of the underlying steps can be combined into a simpler 7-step process[50], focusing the model on the parameters relevant to the efficacy of the ligand therapeutic.

Here, we have adopted the outline of a reduced RME-model developed by Krippendorf et al. [49] for the transferrin cycle in a cell monolayer geometry. The steps described by Ciechanover et al. are listed as follows[51]: iron-saturated Tf (Tf-Fe) binds with the surface receptor (TfR); The Tf-TfR complex then becomes internalized, creating an endosome; The higher pH of the endosome compartment causes Tf-Fe to shed its iron molecules, which are deposited within the cell; The endosome then returns to the cell surface, where the iron-free Tf is released to be reutilized.

Unlike previous models, the geometry and "barrier" effect of the monolayer creates distinguishable apical and basolateral processes and species, designated with "A" and "B" subscript in our adaptation in figure 1. Here, the initial binding of Tf-Fe $[L^+]$ and reversible release occurs at step (1) on the apical side and basolateral side, creating the complex $[RL^+]$. These are then internalized in step (2), where the internalized complex $[RL^+]_i$ sheds the iron molecules through step (3), becoming $[RL]_i$. The surface recycling step occurs in step (4) and proceeds in both basolateral and apical directions. Non-ferrous Tf, $[L]$, is then released in step (5).

Rate equations are derived to track the change of the various molecular species. For instance, the binding of apical Tf-Fe to its receptors in step (1) is written as follows:

$$[R]_A + [L^+]_A \xleftrightarrow{k_1, k_{-1}} [RL^+]_A \quad \text{Eq. 2}$$
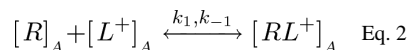
Reaction rates are then applied for the forward and reverse steps, and incorporated into ODEs for each species. For the rate equation of apical Tf-Fe, this is:

$$\frac{d[L^+]_A}{dt} = -k_1 [R]_A \frac{[L^+]_A}{V_A N_A} + k_{-1} [RL^+]_A \quad \text{Eq. 3}$$

All species are expressed in terms of molecules, and the terms $V_A$, which is the volume of the apical chamber, and $N_A$, Avogadro's number, are included to express the free ligand as a

concentration. All reactions are first-order, with the exception of the second-order forward binding steps of Tf-Fe.

Rate constants were obtained from studies of the Tf cycle on the human hematoma line HepG2[41, 52], and are listed in Table 1. The starting conditions were chosen to simulate a typical unidirectional transport study[53]. The ODEs are then solved simultaneously using numerical integration if a number of assumptions are made: (1) the rate kinetics obtained from literature are similar to the those of the cells used in this study, (2) the receptor pool is split evenly between both sides, and (3) there is no receptor degradation or synthesis over the course of a transport study (the number of binding sites remains constant. For further analysis on the validity of these assumptions, please refer to the supplemental text. Ligand-Receptor binding studies were performed to determine the starting concentration of binding sites.

## 4. Results

### 4.1 Number of Receptor Binding Sites

Figure 2 presents the equilibrium binding data of Tf with Caco-2 cells. Non-specific binding in control samples, representing binding through means other than the Tf receptor, increased in proportion with increasing concentration, while specific binding, the difference between the total Tf detected and control samples, levelled off. Non-linear regression analysis of the binding model (Eq. 1) was used to determine both the affinity of the ligand to the receptor, via the association constant $K_a$, and the binding site concentration. The association constant was calculated to be $1.2 \times 10^8 \, M^{-1}$. The binding-site concentration, combined with the known concentration of cells in the binding solution, produced a binding site density of $1.08 \times 10^6$/ cell. For a 12-well transport tray containing approximately 386,000 cells when confluent and fully developed, this would result 323fmol of binding sites per side of the monolayer.

### 4.2 Model Simulation

With all starting conditions accounted for, a monolayer transport simulation was performed assuming an apical concentration of Tf-Fe of 10μg/ml, with the results plotted in Figure 3. The amount of free receptors on the apical side is immediately depleted at the beginning of the experiment due to the strong affinity and quick binding of the ligand at this concentration. The Tf-TfR complexes are then slowly internalized within the cells. This produces an initial sharp increase in internalized endosomes until after 6min, when the endosome concentration decreases as the recycling process becomes significant. Endosomes that accumulate on the basolateral side result in an increase in both basolateral receptors and, once the ligand is released, total basolateral Tf concentrations. Accumulation of basolateral Tf continues until apical receptors are exhausted, plateauing at 320fmol. Apical Tf, distinct from the original Tf-Fe, also accumulates in proportion with basolateral values (not shown in this graph), though receptors returning to this side are then free to transport Tf-Fe again.

*In vitro* transport studies were conducted with the same starting conditions alongside control samples with 100x-fold excess unlabeled Tf-Fe, the results of which are plotted in Figure 4. The excess unlabeled Tf-Fe saturates the available receptor sites, only allowing the labelled ligand to interact with the cell through non-specific mechanisms. These control samples

served three purposes: (1) to verify the integrity of the monolayer, (2) to distinguish between total and RME transport, and (3) to serve as a model for non-specific therapeutic uptake. Control samples resulted in a linear accumulation of Tf in the basolateral chamber, averaging 45±15fmol of total transport. The apparent permeability coefficient ($P_{app}$) was calculated to be $2.9\pm0.8\times10^{-8}$cm/s. This verified that the monolayer was fully developed, as the $P_{app}$ for typical monolayer integrity markers, such as mannitol ($1.2\times10^{-7}$cm/s)[54] or lucifer yellow ($1\times10^{-6}$cm/s)[55], are higher in magnitude. Total transport peaked at 344±27fmol. Specific uptake, determined from the difference between the total and non-specific transport, was found to rise sharply rise before plateauing at 298±22fmol, as expected from the model. This level was below the value predicted by the binding site density study (323fmol). Since levels of apical receptor binding sites correlated with basolateral Tf transport, starting conditions were modified to reflect the new value and the simulations repeated. However, experimental values for basolateral accumulation showed a lag of approximately  t=0.5hr. To compare the results of the two, the output of the model was shifted by  t to overlay with the experimental values.

### 4.3 Dose Study

As many drug delivery assessment methods assume dose proportionality and utilize normalization, we wished to conduct a transport study with a starting apical Tf-Fe concentration of 1μg/ml and 50μg/ml and compare it to the previous 10μg/ml study. The results are plotted in Figure 5. Here, non-specific uptake of the 1 μg/ml study was below our ELISA's detection limit of 10fmol, while uptake of the 50μg/ml study reached as high as 255±18fmol. Specific RME-transport sharply increased in both studies, starting at the time-lag 0.5hr mark, before plateauing after 1.5hr at 293±20fmol with 1μg/ml and 308±34 with 50μg/ml, the differences negligible from the 10μg/ml study.

### 4.3 Short-term Repeat Transport Study

Model simulations indicated that maximum basolateral transport ended with the complete polarization of the available receptor pool: receptors initially on the apical side were deposited to the basolateral side, resulting in an imbalance of receptor distribution. To test how this would impact further transport, consecutive transport studies were conducted with short incubation times (Figure 6) and compared against previous results (Figures 4 and 5). Briefly, the steps are as follows: (1) mock 4hr transport study at 10μg/ml, (2) 2hr incubation in cell culture media, (3) 1hr HBSS incubation, and (4) repeat 4hr transport study at 10μg/ml. Non-specific uptake increased linearly with respect to time, reaching a maximum of 48±9fmol at 4hr. Maximum transport reached 173±9fmol, while specific RME-transport reached a plateau of 126±25fmol, both values significantly lower than the previous 10μg/ml study. To determine the cause of this drop in RME capacity, a model simulation was performed to track the movement of apical receptors across these two studies (Figure 7). As expected, the initial drop in total receptors (bound and unbound) occurs until all 298fmol receptors are exhausted and transport is halted at around the 1hr, followed by the plateau. When the study is halted and culture media is added to both apical and basolateral chambers, the receptors are transported in the reverse direction over the course of 2hrs. However, this only restores approximately 121fmol of receptors. During a further 1hr buffer incubation time, remaining intracellular receptors recycle to each side, resulting in a slight increase of

apical receptor levels to 127fmol, a 58% reduction from initial receptor levels. This results in decreased transport capabilities.

## 4.4 Long-term Repeat Transport Study

Full utilization of the available receptor pool requires their complete saturation over the course of the study. We wished to determine the long-term effects of receptor saturation on the transport capabilities of Tf by growing monolayers in culture media with supplemented human Tf during the tight junction development stage. A transport study with an apical concentration of 10μg/ml was then conducted as done previously (Figure 8). Accumulation of Tf via non-specific uptake reached a maximum of 51±10fmol after 4hrs, while total transport reached a maximum of 300±26fmol. Specific RME transport reached a plateau of 247±38fmol after 1.5hrs, a 17% reduction for our initial 10μg/ml study.

To determine what effects this has on the receptor pool, binding-site analyses were performed on cells grown in the same supplemental media for the same length of time, (Figure 9). Non-linear regression analysis returned new fitting parameters, and showed the cells contained $8.82 \times 10^5$ binding sites/cell. Using Fischer's F-test to test this new parameter on the original data[56], it was determined that the 18% drop in binding sites was significant ($p$=0.0017). In contrast, the new association constant, $1.24 \times 10^8$ M$^{-1}$, was not significantly different from the original value.

# 5. Discussion

## 5.1 Adopted Model

The purpose of using literature RME-models was to gain insight on the important parameters governing the transcytosis across monolayers and how these parameters influence the assessment of drug-delivery devices utilizing this pathway. The model established the importance of the receptor in trafficking Tf across the monolayer, specifically the correlation between basolateral ligand transport and apical receptor concentration. Therefore, trans-monolayer transport capabilities can be estimated using the known receptor pools. We showed two methods that can provide this number: scatchard analyses of binding data and transport studies themselves. Advantages of collecting binding data include the ability to use cells during the growth phase, enabling for faster experiments and larger volumes, and flexibility in culture equipment. High-throughput screening methods have been extensively used for receptor-ligand binding data[57–59], and would ideally be used to screen for more advantageous ligand/cell pairings. Transport studies, despite being limited to specialized Transwell® trays and requiring longer culture periods, provide more direct data for drug-delivery studies, and can be tested alongside passive transport for comparison.

Experimental studies verified the results of the model, though two significant deviations were observed. First, experimental basolateral Tf levels lagged behind the model output by t, indicating the presence of one or more mechanisms not previously accounted for in literature models. Likely, apically internalized endosomes are not immediately available for basolateral recycling, and undergo further mechanisms before undergoing transcytosis. Tf has been found to enter two distinct initial endosome populations which may possess

different recycling mechanisms, though these have not undergone kinetic analyses[60]. Similar lag phenomena have been observed and accounted for in models regarding receptor signalling transduction[61] and virus pathogenesis[62]. However, these modeling methods are used to hide, not explain underlying biological mechanisms[63]. Since the lag did not affect the maximum transport potential and does not factor into the assessment methods being investigated, this was not investigated further.

Second, basolateral Tf levels were 7% lower than levels predicted from the model and receptor-binding studies. This difference can be attributed to the different cell growth stages used between the binding studies, which use cells grown in the exponential growth phase, and transport studies, where cells have entered a non-proliferative stage. Proliferating cells have been previously shown to have increased Tf-receptors levels, presumably due to their higher nutritional iron needs[64, 65], which results in an overestimate of receptors based on binding study results.

As our model includes no cellular mechanism for directing an internalized endosome to specific sides, simulations show that RME results in transport to both sides of the chambers. This is a hindrance to drug delivery devices targeting RME pathways across monolayers, because it is undesirable for ligands to return to the apical chamber, lowering the efficiency of these devices. However, this is typically not observed or reported, as the only distinguishing feature between starting and transported Tf species is the presence of iron. Spectroscopy methods lack the sensitivity to detect this, particularly at high apical concentrations[66], and labeling compounds are most often used to detect only the ligand itself. Radiolabeling methods have previously been used in studies of the Tf cycle to distinguish between iron, using the $^{59}$Fe isotope, and the ligand, using the $^{125}$I isotope[67–70], which could be used here to confirm the results of the model. In addition, this technique could be used to distinguish between passively and RME-transported Tf within the same sample.

## 5.2 Transport Studies

A summary of the results is presented in Table 2, along with commonly observed assessment methods discussed previously: the percentage of dosed Tf to have been transported across via non-specific and combined pathways, the ratio of RME to passive transport ratio, and the total to passive transport ratio.

In comparing the results for non-specific transport in the variably dosed studies, we observed significant differences among their basolateral Tf accumulation, though when normalized to their applied dose, they showed no significant differences among them; this demonstrates the property of dose-proportionality, which implies that at any given time point above zero

$$[L]_B \propto dose\,(\text{non−specific}) \quad \text{Eq. 4}$$

where $[L]_B$ in this case only relates to non-specific transport. In the repeat dose studies, non-specific transport in both the short-term and long-term study demonstrated dose-

proportionality as well, despite observed drops in receptor concentration. This demonstrates that the receptor has no influence on non-specific transport across the monolayer. Preliminary studies using media cooled to 4°C in controls, which shuts down ATP-driven processes, indicated that other active transport pathways were not a factor, and diffusion through the monolayer was the predominant mechanism behind non-specific transcytosis (data not shown).

In contrast, RME-transport remained unchanged in the variable dose studies, despite the changes in apical Tf concentration. This is because Tf outnumbered available receptors in all cases, making the receptor pool the limiting factor in specific transport. This mechanism leads to a lack of dose-proportionality, and is a common cause for nonlinear pharmacokinetics[71].

The repeat use of ligand transport was shown to adversely affect the available receptor pool on cells, decreasing RME- and overall transport. Short-term studies were designed to mimic dose-regiments requiring multiple daily uses of RME-drug delivery devices. Simulations showed that receptors travel to and from the basolateral side during the transport and equilibrium steps, but when equilibrium times were cut short, subsequent transport was 42% of its initial amount due to diminished apical receptor levels. Muro et al. had similarly found the slow recycling of the adhesion molecule ICAM-1 to result in diminished intracellular transport of drug delivery vehicles after short, successive dosing, but had believed ligands with faster transit times, like Tf, would be immune to this effect[72]. However, due to the geometry of the monolayer and the longer than expected transcellular recycling times, this was found not to be the case.

Long-term studies, designed to mimic continuous use of an RME-therapeutic system, also resulted in diminished transport (247±38). Accompanying binding-site analyses demonstrated that this is caused by a decrease in receptor pools. Previously, cells have shown to down-regulate their Tf-receptor levels in iron-rich culture media[50, 73, 74], while conversely up-regulating their receptor levels when deprived of iron[75, 76], which serves to control the uptake of iron in response to different environmental conditions. Originally, the source for iron is the endogenouse bovine-Tf present in the culture media, which has an affinity 165-fold less than that of human-Tf[77]. Furthermore, endogenous Tf levels are a mixture of diferric-, monoferric, and apo-Tf, with the latter two having affinities 4.4-fold less and 24-fold less than that of diferric-Tf, respectively[78]. In total, diferric-Tf typically only represent 10% of plasma Tf concentrations[79]. Thus, the addition of human differic-Tf to the culture media provides a much more potent iron transporter than endogenous bovine-Tf level, resulting in receptor down-regulation. This feedback system is not exclusive to monolayer cell geometries, and affects surface and intra-cellular targeting devices as well. Thus, the efficacies of RME-based drug delivery devices are dependent on their dose regiment.

The dependence of the receptor in RME-transport processes, while having no role in passive ones, produces misleading results when directly comparing the two. When calculating the percentage of the available ligand that had been transported across the monolayer, the 1μg/ml study appears to have the superior result, despite similar performances in the RME

transport process. The ratios of RME/passive and total/passive transport increases similarly with decreasing dose concentrations because the receptor availability remains unchanged. On the other hand, RME-transport levels decreased in both short- and long-term repeat studies due to drops in receptor levels, while consistent apical ligand concentrations resulted in unchanging passive-transport levels. This also produces results that appear inferior to the original 10μg/ml study, according to all three assessment methods, despite the studies receiving the same apical dose.

Furthermore, studies that only observe the total transport of RME-therapeutic drug delivery systems without proper controls fail to recognize that this is the result of the RME and non-specific pathways occurring in tandem. Comparing these to the passive transport of the therapeutics will produce one of two outcomes: if the contribution of RME-transport is low, total transport will not appear different from the therapeutic alone; if RME-transport is significant, total transport will appear greater than the therapeutic. Thus, this method may not only be misleading, but also incapable of producing an inferior result.

## 6. Conclusions

The disagreements among the results in Table 2 highlight the fallacy in directly comparing passively transported therapeutics and RME-based therapeutic systems: ligand/receptor systems do not improve the passive uptake of therapeutics across monolayers; on the contrary, they occur within separate and independent transport routes. In this study, we demonstrated how a typical RME-drug delivery device is transported across a monolayer through both mechanisms simultaneously: (1) non specific-uptake, which occurs in a dose-proportional manner, allowing for the use of dose-normalized concentration measurements[80, 81], and (2) the endocytosis pathways, which was shown to lack dose-proportionality, and invalidating the assumptions inherent in typical assessment methods. The availability of receptors, and thus the performance of the delivery device, was further shown to change with repeated use of the cycle. Thus, while it is clear that RME systems have the potential to improve the overall transport of therapeutics, it is imperative that future research of these devices be evaluated within the context of the ligand and receptor's capabilities and pharmacokinetics. These capabilities were predicted using simple receptor-binding studies, which should be explored to screen for higher performing RME combinations.

## Supplementary Material

Refer to Web version on PubMed Central for supplementary material.

## Acknowledgments

# References

1. Pardridge WM. Drug discovery today. 2007; 12:54. [PubMed: 17198973]

2. Sahoo SK, Labhasetwar V. Molecular pharmaceutics. 2005; 2:373. [PubMed: 16196490]

3. Jones AR, Shusta EV. Pharm Res. 2007; 24:1759. [PubMed: 17619996]

4. Yezhelyev MV, et al. The lancet oncology. 2006; 7:657. [PubMed: 16887483]

5. Gao X, et al. Nat Biotechnol. 2004; 22:969. [PubMed: 15258594]

6. Artemov D, et al. Magnetic resonance in medicine : official journal of the Society of Magnetic Resonance in Medicine / Society of Magnetic Resonance in Medicine. 2003; 49:403.

7. Murray JC, Moghimi SM. Critical reviews in therapeutic drug carrier systems. 2003; 20:139. [PubMed: 14584522]

8. Ruoslahti E. Drug discovery today. 2002; 7:1138. [PubMed: 12546857]

9. Moghimi SM, et al. FASEB journal : official publication of the Federation of American Societies for Experimental Biology. 2005; 19:311. [PubMed: 15746175]

10. Pan X, Lee RJ. Expert Opin Drug Deliv. 2004; 1:7. [PubMed: 16296717]

11. Ferrari M. Trends in biotechnology. 2010; 28:181. [PubMed: 20079548]

12. Allen TM. Nature reviews Cancer. 2002; 2:750.

13. Sudimack J, Lee RJ. Adv Drug Deliv Rev. 2000; 41:147. [PubMed: 10699311]

14. Muro S. J Control Release. 2012; 164:125. [PubMed: 22709588]

15. Russell-Jones GJ. Adv Drug Deliv Rev. 1996; 20:83.

16. Olivier JC. NeuroRx : the journal of the American Society for Experimental NeuroTherapeutics. 2005; 2:108. [PubMed: 15717062]

17. Andrieux K, Couvreur P. Wiley interdisciplinary reviews Nanomedicine and nanobiotechnology. 2009; 1:463. [PubMed: 20049811]

18. Kavimandan NJ, et al. Biomaterials. 2006; 27:3846. [PubMed: 16529810]

19. Shofner JP, et al. Macromolecular bioscience. 2010; 10:299. [PubMed: 20034125]

20. Shah D, Shen WC. Journal of pharmaceutical sciences. 1996; 85:1306. [PubMed: 8961144]

21. Ragnaill MN, et al. Eur J Pharm Biopharm. 2011; 77:360. [PubMed: 21236340]

22. Wagner S, et al. PLoS One. 2010; 5:e14213. [PubMed: 21151975]

23. Widera A, et al. Pharm Res. 2004; 21:278. [PubMed: 15032309]

24. Habberfield A, et al. International journal of pharmaceutics. 1996; 145:1.

25. Zhu ZB, et al. Virology. 2004; 325:116. [PubMed: 15231391]

26. Saito Y, et al. Proc Natl Acad Sci U S A. 1995; 92:10227. [PubMed: 7479757]

27. Ulbrich K, et al. Eur J Pharm Biopharm. 2009; 71:251. [PubMed: 18805484]

28. Amet N, et al. J Control Release. 2010; 141:177. [PubMed: 19761807]

29. Xia CQ, et al. The Journal of pharmacology and experimental therapeutics. 2000; 295:594. [PubMed: 11046093]

30. Chalasani KB, et al. J Control Release. 2007; 122:141. [PubMed: 17707540]

31. Chalasani KB, et al. J Control Release. 2007; 117:421. [PubMed: 17239471]

32. Tuesca A, et al. Journal of pharmaceutical sciences. 2008; 97:2607. [PubMed: 17876768]

33. Klausner RD, et al. Journal of Biological Chemistry. 1983; 258:4715. [PubMed: 6300098]

34. Hermanson, GT. Bioconjugate Techniques. 2. Academic Press; London, UK: 2008.

35. Green, NM. Spectrophotometric determination of avidin and biotin. In: Donald, BM.; Lemuel, DW., editors. Methods in Enzymology. Academic Press; 1970. p. 418

36. Vieira A. Mol Biotechnol. 1998; 10:247. [PubMed: 9951704]

37. Podbilewicz B, Mellman I. The EMBO journal. 1990; 9:3477. [PubMed: 2209555]

38. Motulsky, HJ.; Christopoulos, A. Fitting models to biological data using linear and nonlinear regression. GraphPad Software Inc; San Diego CA: 2003. www.graphpad.com

39. Brown AM. Computer methods and programs in biomedicine. 2001; 65:191. [PubMed: 11339981]

40. Orton RJ, et al. The Biochemical journal. 2005; 392:249. [PubMed: 16293107]

41. Ciechanover A, et al. Journal of Biological Chemistry. 1983; 258:9681. [PubMed: 6309781]

42. Ghaghada KB, et al. J Control Release. 2005; 104:113. [PubMed: 15866339]

43. Shankaran H, et al. PLoS computational biology. 2007; 3:e101. [PubMed: 17542642]

44. Ghosh RN, et al. Journal of cell science. 1994; 107(Pt 8):2177. [PubMed: 7983176]

45. Starbuck C, Lauffenburger DA. Biotechnology progress. 1992; 8:132. [PubMed: 1368006]

46. Lund KA, et al. The Journal of biological chemistry. 1990; 265:15713. [PubMed: 1975591]

47. Kholodenko BN, et al. The Journal of biological chemistry. 1999; 274:30169. [PubMed: 10514507]

48. Schoeberl B, et al. Nat Biotechnol. 2002; 20:370. [PubMed: 11923843]

49. Krippendorff BF, et al. J Pharmacokinet Pharmacodyn. 2009; 36:239. [PubMed: 19554432]

50. Kato Y, et al. Journal of Controlled Release. 1996; 39:191.

51. Ciechanover A, et al. Journal of cellular biochemistry. 1983; 23:107. [PubMed: 6327736]

52. Dautry-Varsat A, et al. Proceedings of the National Academy of Sciences. 1983; 80:2258.

53. Descamps L, et al. The American journal of physiology. 1996; 270:H1149. [PubMed: 8967351]

54. Hubatsch I, et al. Nature protocols. 2007; 2:2111.

55. Acharya P, et al. Drug metabolism and disposition: the biological fate of chemicals. 2008; 36:452. [PubMed: 17967933]

56. Motulsky HJ, Ransnas LA. FASEB journal : official publication of the Federation of American Societies for Experimental Biology. 1987; 1:365. [PubMed: 3315805]

57. Zeng H, et al. Chembiochem. 2013; 14:827. [PubMed: 23585185]

58. Hulme EC, Trevethick MA. British Journal of Pharmacology. 2010; 161:1219. [PubMed: 20132208]

59. Szyma ski P, et al. International Journal of Molecular Sciences. 2011; 13:427. [PubMed: 22312262]

60. Lakadamyali M, et al. Cell. 2006; 124:997. [PubMed: 16530046]

61. Coombs, D., et al. A Review of Mathematical Models for T Cell Receptor Triggering and Antigen Discrimination. In: Molina-Parais, C.; Lythe, G., editors. Mathematical Models and Immune Cell Biology. Springer; New York: 2011. p. 25

62. Nelson PW, et al. Mathematical biosciences. 2000; 163:201. [PubMed: 10701304]

63. Forde, JE. Delay Differential Equation Models in Mathematical Biology. Department of Mathematics, University of Michigan, University of Michigan; 2005.

64. Larrick JW, Cresswell P. Journal of supramolecular structure. 1979; 11:579. [PubMed: 232525]

65. Frazier JL, et al. J Clin Invest. 1982; 69:853. [PubMed: 6804495]

66. Stoscheck, CM. [6] Quantitation of protein. In: Murray, PD., editor. Methods in Enzymology. Academic Press; 1990. p. 50

67. Chitambar CR, Seligman PA. J Clin Invest. 1986; 78:1538. [PubMed: 3465751]

68. Davis RJ, Czech MP. The EMBO journal. 1986; 5:653. [PubMed: 3011419]

69. Alvarez-Hernandez X, et al. Biochim Biophys Acta. 1991; 1070:205. [PubMed: 1751528]

70. Girones N, Davis RJ. The Biochemical journal. 1989; 264:35. [PubMed: 2604716]

71. Ludden TM. Clin Pharmacokinet. 1991; 20:429. [PubMed: 2044328]

72. Muro S, et al. Blood. 2005; 105:650. [PubMed: 15367437]

73. Ward JH, et al. The Journal of biological chemistry. 1982; 257:10317. [PubMed: 6286649]

74. Pelicci PG, et al. FEBS letters. 1982; 145:350. [PubMed: 6290272]

75. Bomford A, et al. The Biochemical journal. 1986; 236:243. [PubMed: 3790074]

76. Bridges KR, Cudkowicz A. The Journal of biological chemistry. 1984; 259:12970. [PubMed: 6092356]

77. Young SP, Garner C. The Biochemical journal. 1990; 265:587. [PubMed: 2302189]

78. Young SP, et al. The Biochemical journal. 1984; 219:505. [PubMed: 6743230]

79. Lane RS. British journal of haematology. 1975; 29:511. [PubMed: 1191562]

80. Eisenblaetter, T.; Teichert, L. Dose Linearity and Proportionality. In: Vogel, HG., et al., editors. Drug Discovery and Evaluation: Methods in Clinical Pharmacology. Springer; Heidelberg: 2011.

81. Smith, BP. Assessment of Dose Proportionality. In: Bonate, P.; Howard, D., editors. Pharmacokinetics in Drug Development: Clinical Study Design and Analysis. Springer New York; New York: 2004. p. 363
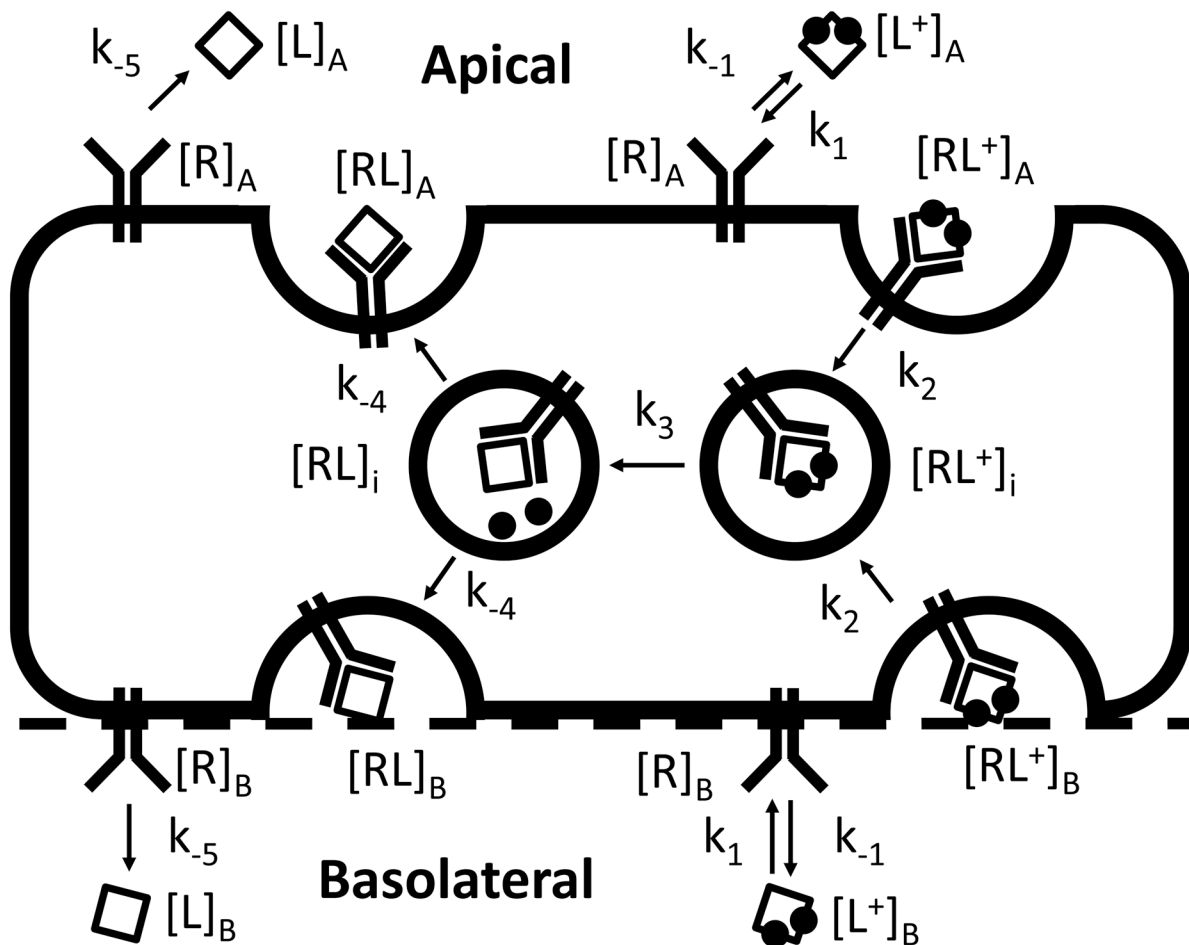
**Figure 1.**
Transferrin cycle in a cell monolayer geometry. Subscripts "A" and "B" denote apical and basolateral species, respectively. The "+" superscript indicates full iron saturation of Tf. Steps
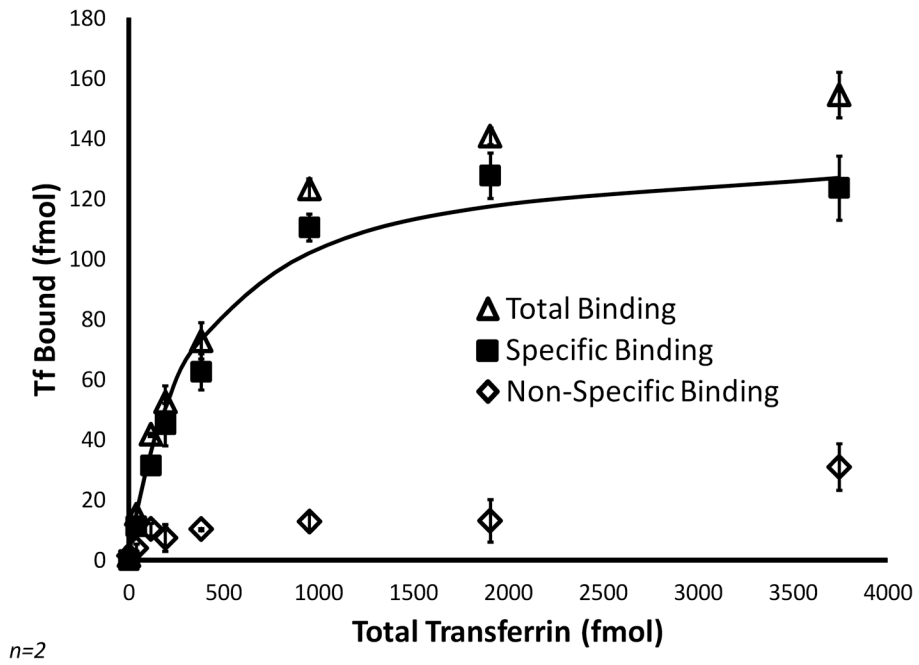
**Figure 2.**
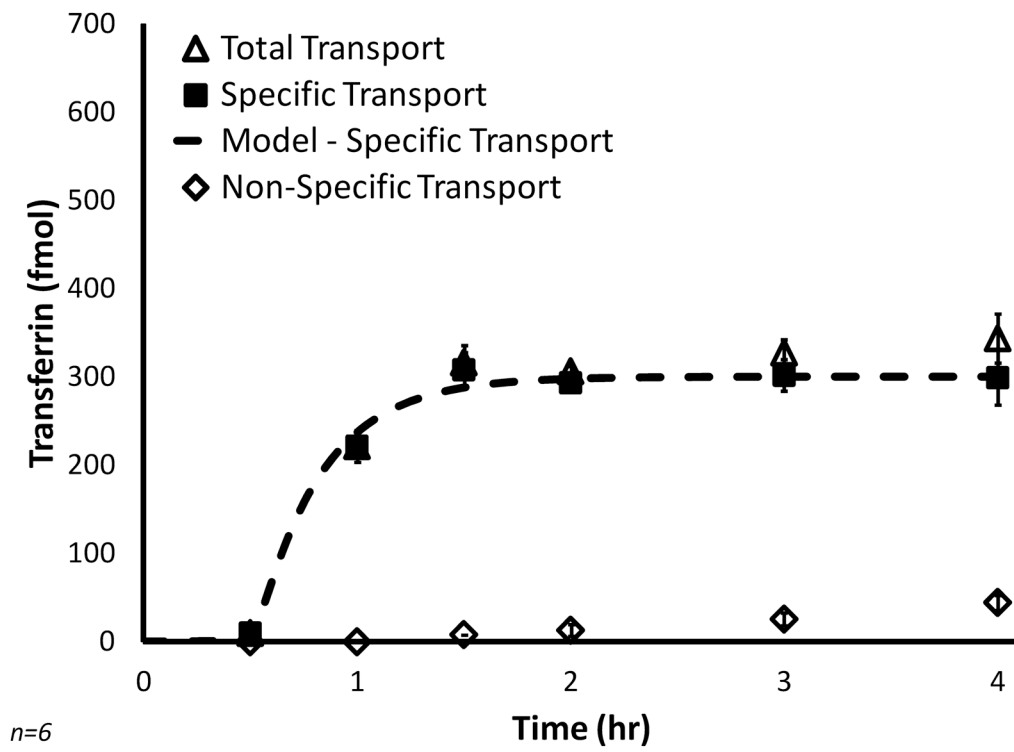Receptor-ligand binding data of Tf to CaCo-2 cells
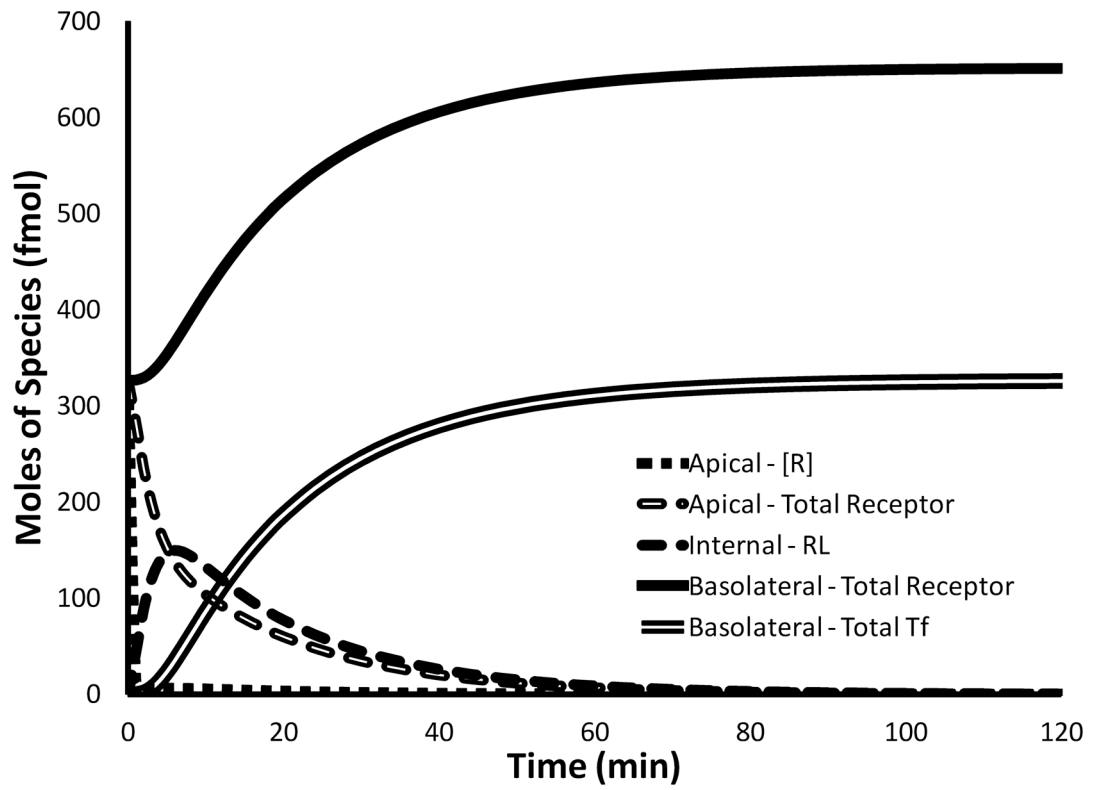
**Figure 3.**
Model simulation of Tf transport across CaCo-2 monolayer at 10μg/ml apical concentration
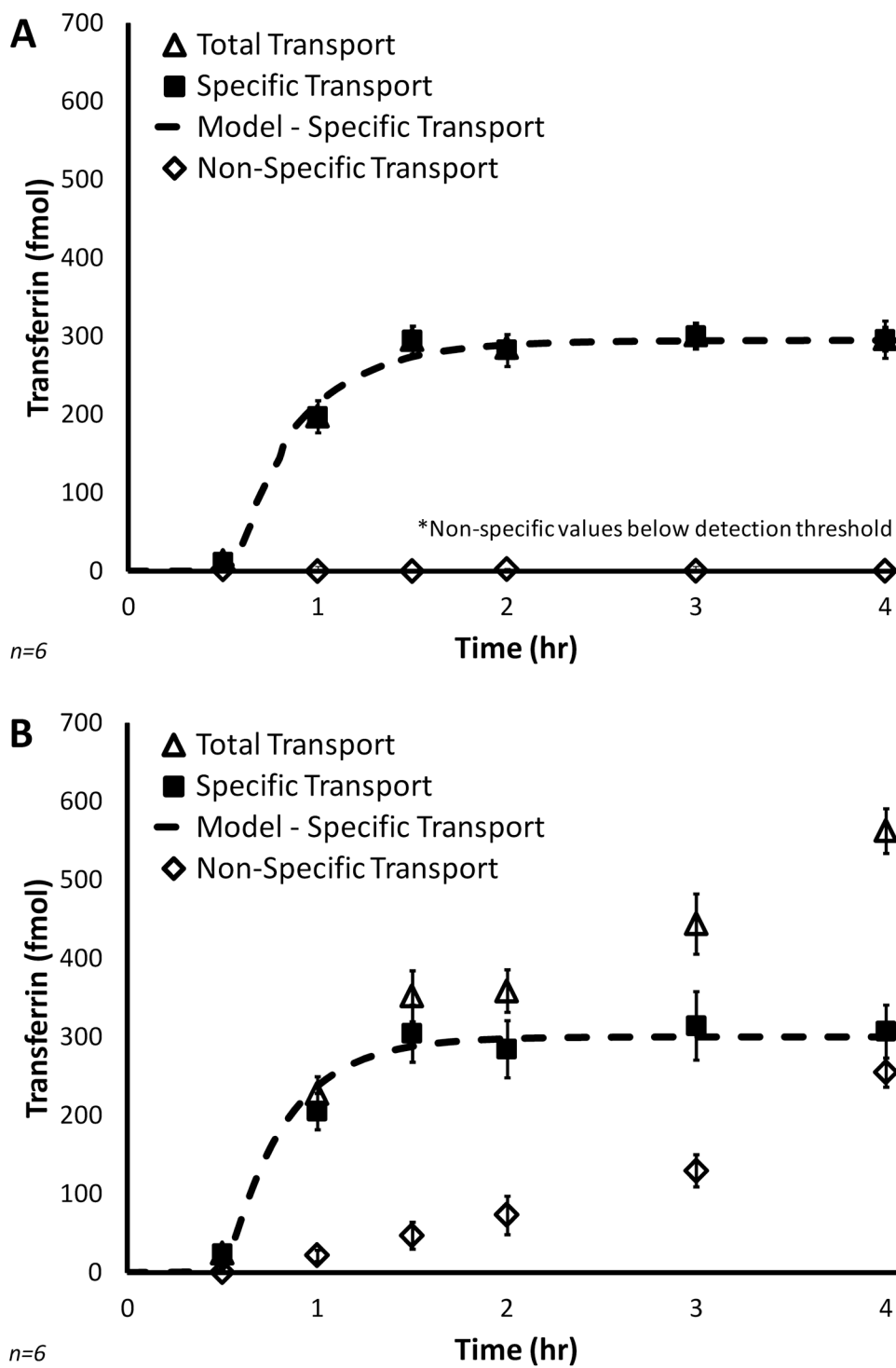
**Figure 4.**
Transport study at 10μg/ml Tf-Fe

**Figure 5.**
(A) Transport study at 1μg/ml Tf-Fe
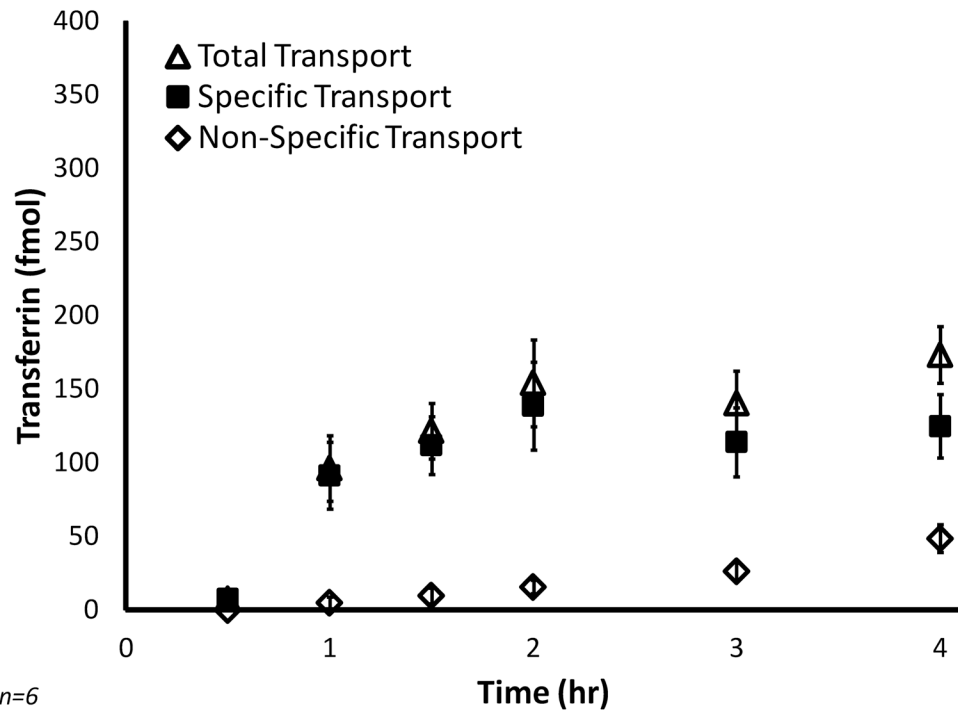(B) Transport study at 50μg/ml Tf-Fe
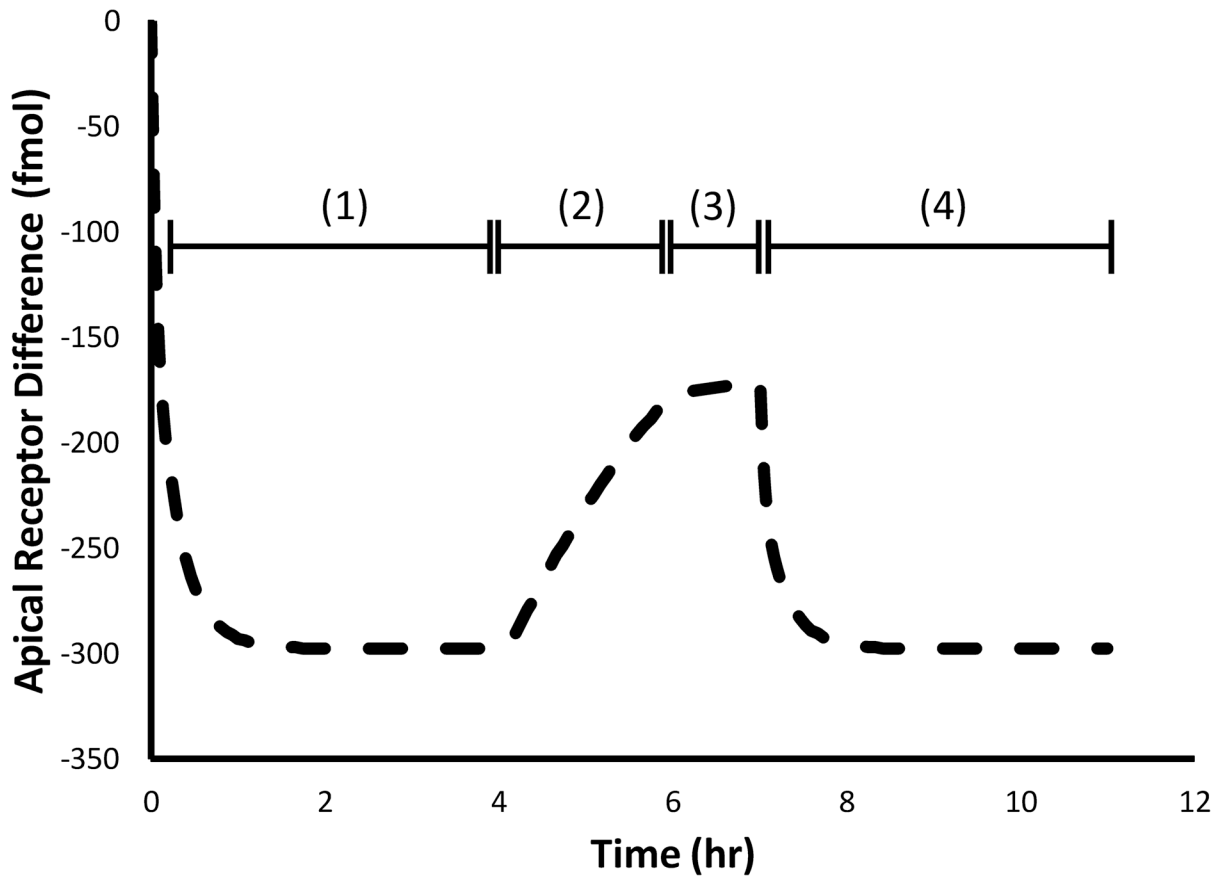
**Figure 6.**
Short-term repeat study

**Figure 7.**
Model simulation of apical receptor levels (difference from starting point). The stages shown are: (1) Initial 4hr transport study, (2) 2hr culture media equilibration, (3) 1hr Buffer equilibration, and (4) repeated 4hr transport study
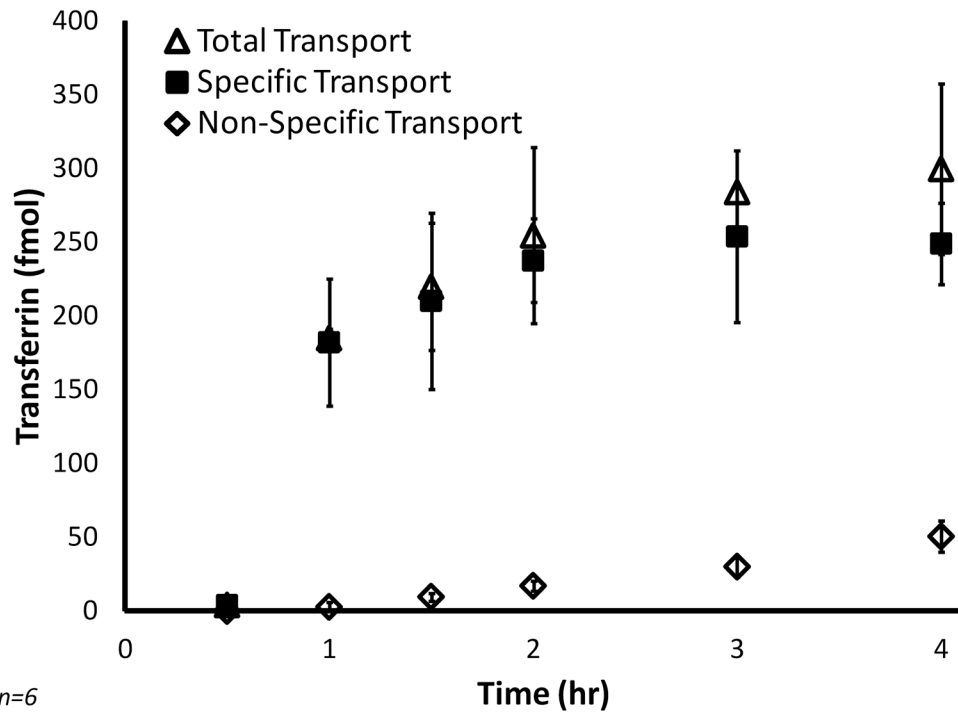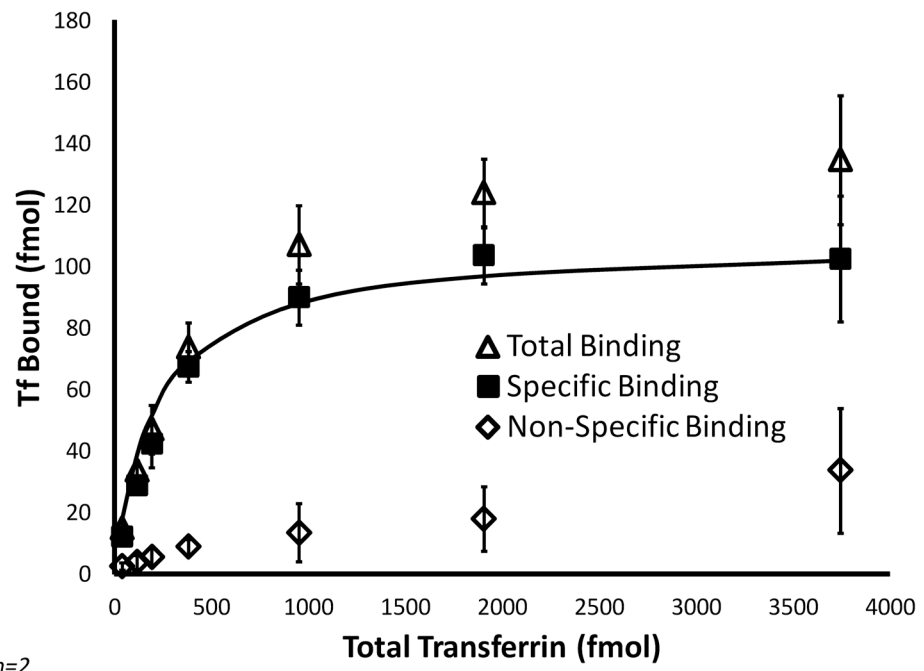
**Figure 8.**
Long-term transport study

*n=2*

**Figure 9.**
Long-term receptor-ligand binding data of Tf to CaCo-2 cells

**Table 1**

Kinetic Parameters

| Parameter | Rate constant | Value |
|---|---|---|
| Binding of [$L^+$] | $k_1$ ($mol^{-1}$ $min^{-1}$) | 3.02 x $10^6$ |
| Dissociation of [$RL^+$] | $k_{-1}$ ($min^{-1}$) | 0.09 |
| Internalization of [$RL^+$] | $k_2$ ($min^{-1}$) | 0.20 |
| Loss of iron[a] | $k_3$ ($min^{-1}$) | 0.28 |
| Recycling of [RL]$_i$[a] | $k_{-4}$ ($mol^{-1}$ $min^{-1}$) | 0.28 |
| Dissociation of [LR] | $k_{-5}$ ($min^{-1}$) | 2.60 |

[a]From Ciechanover et al.[41], The iron-loss and recycling step are known to combine so that $1/0.14 = 1/k_3 + 1/k_{-4}$. These rates were assumed to be equal for the sake of the simulation.

**Table 2**

Transport Assessment

| | Variable Dose Studies | | | Repeat Studies | |
| --- | --- | --- | --- | --- | --- |
| | | | | Short-term | Long-term |
| Dose (μg/ml) | 10 | 1 | 50 | 10 | 10 |
| *Transport* | | | | | |
| Total ($t_{4hr}$) (fmol) | 344±27 | 293±20 | 563±28 | 173±9 | 300±26 |
| RME (fmol) | 298±22 | 293±20 | 308±34 | 126±25 *** | 247±38 *** |
| Passive ($t_{4hr}$) (fmol) | 45±15 | <10 (4[†]) *** | 255±18 *** | 48±9 | 51±10 |
| *Analysis* | | | | | |
| % Transported - Passive | 0.082 | <0.16 (0.07[†]) | 0.075 | 0.077 | 0.082 |
| % Transported - Combined | 0.52 | 4.7 | 0.18 | 0.20 | 0.40 |
| RME/Passive | 6.7 | >30 (60[†]) | 1.2 | 2.6 | 4.9 |
| Total/Passive | 7.7 | >30 (60[†]) | 2.2 | 3.6 | 5.9 |

Analyses used total and passive transport values at the 4hr mark

[†] Results below lower detection threshold. Value in parentheses is an estimate based on $P_{app}$ of other studies' control results.

*** Results show a significant difference with *p<0.001*.